Medium term high frequency observation of discharges and suspended sediment in a Mediterranean mountainous catchment

M. Esteves, C. Legout, O. Navratil, O. Evrard

MEDIUM TERM HIGH FREQUENCY OBSERVATION OF DISCHARGES AND SUSPENDED SEDIMENT IN A MEDITERRANEAN MOUNTAINOUS CATCHMENT.

M. ESTEVES (1), C. LEGOUT (2), O. NAVRATIL (3), O. EVRARD (4)

(1) Institut des Géosciences de l'Environnement (IGE) - Université Grenoble Alpes/ IRD, BP 53, 38041-Grenoble Cedex 9 (France)

(2) Institut des Géosciences de l'Environnement (IGE) - Université Grenoble Alpes, BP 53, 38041-Grenoble Cedex 9 (France)

(3) Univ Lyon, Université Lumière Lyon 2, CNRS, UMR 5600 EVS, F-69635 Lyon (France)

(4) Laboratoire des Sciences du Climat et de l'Environnement, LSCE/IPSL, Unité Mixte de Recherche 8212 (CEA-CNRS-UVSQ), Université Paris-Saclay, F-91198 Gif-sur-Yvette (France)

Correspondance to: M. Esteves, Institut des Géosciences de l'Environnement, UMR 5001, UGA, CS 40 700, 38058 Grenoble cedex 9

Ph: (0033) 4 76 51 49 62

Fax: (0033) 4 76 63 58 87

E-mail: michel.esteves@ird.fr

Short title: Medium term high frequency observation of suspended sediment

Keywords: Erosion, turbidity, sediment yield, sediment transport, French Mediterranean Alps

Abstract

In mountainous catchments, soil erosion and sediment transport are highly variable throughout time and their quantification remains a major challenge for the scientific community. Understanding the temporal patterns and the main controls of sediment yields in these environments requires a long term monitoring of rainfall, runoff and sediment flux. This paper analyses this type of data collected during 7 years (2007 – 2014), at the outlet of the Galabre River, a 20 km² watershed, in south eastern France, representative of meso-scale Mediterranean mountainous catchments.

This study is based on a hybrid approach using continuous turbidity records and automated total suspended solid sampling to quantify the instantaneous suspended sediment concentrations (SSC), sediment fluxes, event loads and yields. The total suspended sediment yield was 4661 Mg km^{-2} and was observed during flood events. The two crucial periods for suspended sediment transport at the outlet were June and November/December (63 % of the total). The analysis of suspended sediment transport dynamics observed during 236 flood events highlighted their intermittency and did not show any clear relationship between rainfall, discharge and SSC. The most efficient floods were characterised by counter-clockwise hysteresis relationships between SSC and discharges. The floods with complex hysteresis were the more productive in the long term, during this measuring period exceeding a decade. Nevertheless, the current research outlines the need to obtain medium-term (five years) continuous time series to assess the range of variations of suspended sediment fluxes and to outline clearly the seasonality of suspended sediment yields. Results suggest the occurrence of a temporal dis-connectivity in meso-scale catchments over short time-scales between the meteorological forcing and

the sediment yields estimated at the outlet. These findings have important methodological impacts for modelling and operational implications for watershed management.

1. INTRODUCTION

In catchments equipped with hydroelectric power plants, improving the knowledge on water availability and Suspended Sediment (SS) dynamics are crucial issues for reservoir and environmental management, and they remain significant challenges for scientists (Wood and Armitage, 1997; Valero-Garcés *et al.*, 1999; Owens *et al.*, 2005). The suspended load is mainly composed by particles with a diameter lower than that of sand (<2 mm), and it comprises typically silt and clay-sized material (<63% µm; Walling and Moorehead, 1989). Usually, this sediment transport process provides the main pathway for the exportation of the sediment load (Lenzi et al., 2003; Alexandrov *et al.*, 2009; Turowski *et al.*, 2010). In mountainous areas, hillslope erosion and mass movements supply large quantities of suspended sediment to rivers (Tropeano, 1991; Milliman and Syvitski, 1992; Dedkov and Moszheirn, 1992; Lenzi and Marchi, 2000; Korup *et al.*, 2004; Cuomo *et al.*, 2015). Rainfall, runoff and sediment transport are highly variable in space and time (Alvera and Garcia-Ruiz, 2000; Meybeck *et al.*, 2003; Schmidt and Morche 2006; Mano *et al.*, 2009; Evrard *et al.*, 2011; Navratil *et al.*, 2012). In addition, a major part of the sediment load is transported during very short time periods corresponding to a limited number of storm events (Alvera and Garcia-Ruiz, 2000; Schmidt and Morche 2006; Zabaleta *et al.*, 2007; Navratil *et al.*, 2012; Tuset *et al.*, 2015). Accordingly, the high-frequency observation of Suspended Sediment Concentration (SSC) is required to provide reliable estimates of Suspended Sediment Yields (SSY). The quantification of SSC in samples collected during occasional samplings only may lead to large errors in SSY estimates (Thomas and Lewis, 1993; Phillips *et al.*, 1999; Coynel *et al.*, 2004; Moatar *et al.*, 2006, Skarbøvik *et al.*, 2012). To avoid this problem, continuous turbidity measurements are currently used as a surrogate variable for SSC quantification (Foster *et al.*, 1992; Lewis, 1996, Wass and Leeks, 1999; Lenzi *et al.*, 2003; Brasington and Richards, 2000; Orwin and Smart, 2004; Stott and Mount, 2007; Mano *et al.*, 2009; López-Tarazón *et al.*, 2009; Navratil *et al.*, 2011). SSC are then estimated through the determination of a calibration relationship between turbidity and SSC based on the analysis of suspended sediment samples collected during flood events. This method remains the easiest and the most widely used for high-frequency observation of suspended sediment (Riley, 1998; Wren *et al.*, 2000; Pfannkuche and

Schmidt, 2003; Downing, 2006; Gray and Gartner, 2009; Navratil *et al.*, 2011, Slaets *et al.*, 2014; Ziegler *et al.*, 2014).

Given the high variability of SSY at both annual and flood event scales, many studies strived to identify the factors controlling SSY. The temporal and spatial patterns of precipitation (Regües and Gallart, 2004; Garcia-Ruiz *et al.*, 2005; Nadal-Romero *et al.*, 2014), the runoff regimes (Dedkov and Moszherin, 1992; Nadal-Romero *et al.*, 2008; Mano *et al.*, 2009; Grangeon *et al.*, 2012; López-Tarazón and Batalla, 2014; Tuset *et al.*, 2015), the peak discharge (Gao and Josefson, 2012), groundwater storage variations (Duvert *et al.*, 2011; Tolorza *et al.*, 2014) and sediment transfer processes (storage vs. mobilization) within the basin (López-Tarazón *et al.*, 2010; Evrard *et al.*, 2011; Park and Hunt, 2017) or in the vicinity of streams (Lefrançois *et al.*, 2007; Salant *et al.*, 2008; Gourdin *et al.*, 2014) were identified as the key factors governing SSY in small catchments.

Most of these previous studies analysed short-term (2 to 3 years) SSY time-series or focused on the flood event scale, in particular when investigating the relationship between SSC and water discharges (Williams, 1989). Very often, a lag was observed between the maximum of SSC and that of water discharge (Asselman, 1999; Sadeghi *et al.*, 2008; Gao and Josefson, 2012; Aich *et al.*, 2014). Hysteresis patterns are often complex and their understanding can be complicated. Indeed, SSC does not only vary with discharge, but also with the sources supplying particles and their availability in the channel or on nearby hillslopes, which are greatly affected by factors such as climate, relief, soil types, channel size or land cover (Vanmaercke *et al.*, 2012).

At the light of these difficulties, very few studies have been conducted on longer term (5 to 10 years) SSY time-series, although the continuous monitoring of suspended sediment dynamics during long periods remains of prime importance to analyse seasonal cycles and medium-term trends (Vanmaercke *et al.*, 2012). These issues are crucial for hydroelectric power plant managers because sediment often accumulates in water reservoirs by siltation (Morris and Fan, 1998; Walling and Fang, 2003; Renwick *et al.*, 2005; Lee and Foster, 2013). As reservoir dredging is a very expensive management operation, understanding and predicting the different factors controlling SSY are of paramount importance to design appropriate and effective control measures and management procedures in headwater catchments (Morris and Fan, 1998; Bogen and Bønsnes, 2005, Morris, 2014). Choosing the appropriate location and technique to design erosion control measures on hillslopes requires long-term records in order to cover both the seasonal and the interannual variability of SSY.

This study was based on a 7 years dataset (from October 2007 to December 2014) of streamflow and suspended sediment concentrations monitored in a 35 km² mountainous river catchment, the Galabre River in the Southern French Pre-Alps. The objective of the current study was to analyse the physical processes controlling the temporal variability of suspended sediment yields. The specific goals of this paper where therefore (i) to quantify sediment loads and yields; (ii) to analyse their sensitivity to the length of the time-series; (iii) and to provide further insight into the temporal variability of suspended sediment loads. This work will improve our understanding of suspended sediment dynamics in an Alpine Mediterranean catchment that is representative of similar basins found in this region.

2. MATERIALS AND METHODS

2.1. Catchment description

The Galabre River (lat.: 44°11′49″N, long.: 06°12′57″E) is a headwater tributary of the Bléone River that flows into the Rhône River, France (total drainage area, 34.8 km²; Figure 1a). In 2007, hydro-sedimentary monitoring was initiated in the 20 km² upstream part of the Galabre river basin where elevations range from 735 m to 1909 m. The catchment length is 7 km. The geological bedrock is composed of various sedimentary rocks (Figure 1b), limestones (34%), marls and marly limestones (30%), gypsum (9%), molasses (9%) and Quaternary deposits (18%) resulting in a badland topography, extensive gully development and high transfer of sediment. The hillslopes are overlain by thin soils with a depth lower than 0.50 m and exhibiting a high degree of stoniness. Highly erodible zones covering 9.5% of the catchment are scattered across the entire catchment area. The catchment is part of the Draix Bléone research observatory belonging to the French network of Critical Zone Observatories (OZCAR, Gaillard *et al.*, 2018).

The climate of the study area is both Mediterranean and mountainous, and characterized by a pronounced seasonality with the occurrence of frost in winter and high-intensity rainfall in summer. Mean annual temperature is 12°C at 400 m ASL (above sea level), with a high temperature amplitude between summer and winter (approximately 18°C at a monthly timescale). Average annual precipitation reaches around 1000 mm. Rainfall is characterised by high seasonal variations, with a maximum in spring and autumn with respectively 27% and 32% of the total (Navratil *et al.*, 2012). Evapotranspiration leads to a water deficit well marked from July to October.

Six different land covers are found in the Galabre catchment (Figure 1c). Upper catchment parts are mainly covered with forests (52%), scrubland (30 %), sparse vegetation (12 %) and grassland (3%) while the lower part of the study area is mainly occupied by agricultural land and sparse urban areas. The human impact in the catchment therefore remains very low.

The flow in the main river network is perennial, although very low discharges (0.02 $m^3 s^{-1}$) can be measured during low-flow periods in summer.

2.2. Field data acquisition

Three main data sets were collected in the catchment: the flow discharge, the suspended and sediment concentration were measured with a 10 minutes time step whereas the precipitation was continuously recorded.

A river measuring station was installed at the outlet of the Galabre catchment in September 2007 and equipped with a 24-GHz radar (Paratronic Cruzoe®) to measure the water level. Flow discharges were regularly gauged with the salt (NaCl) dilution method and a current flow meter. A water-level discharge rating curve was established from 35 flow discharges measured from 2007 to 2014 (ranging from 0.017 $m^3 s^{-1}$ to 0.948 $m^3 s^{-1}$) and an extrapolation performed by hydraulic modelling (HEC-RAS). The surveyed cross-section was very stable (i.e. bedrock cross-section without sedimentation or erosion). Owing to the difficulty of sampling during high discharges, a higher level of uncertainty is expected for discharge estimates during these periods (Navratil et al.; 2011).

A nephelometric turbidimeter (WTW Visolid® 700-IQ) and a IQ182 sensor net transmitter measured the turbidity in the water flow by infra-red light (860 nm) 90°-diffusion (for low concentrations) and backscattering (for high concentrations). The sensor was designed to measure high suspended sediment concentrations in rivers and wastewater treatment plants. Ultrasonic cleaning of the sensor during the measurement prevents fouling with organic and fine sediment. To avoid any bias with natural solar light, the sensor was oriented downward (angle, approximately 30°) in the upstream direction of the river flow and 20 cm above the river bottom. The turbidimeter was also exposed to calcification resulting in calcareous precipitation on the optic cell. To prevent this problem, it was cleaned every two months with 5% HCl acid.

Every 10 min, a data logger (Campbell® CR800) recorded the water level and the turbidity for 1 min. with a 1 Hz frequency and calculated the basic signal statistics: the

mean turbidity $\overline{T}$ and water level $\overline{H}$, the standard deviations (respectively, σ_T and σ_H) and the minimum and maximum values. Data integration during a 1-min time-step was found to provide a good compromise between the short time-scale fluctuations of the signals and their variations at the flood event scale (a few hours in this case study). Statistics were then downloaded daily *via* GSM transmission and stored at the laboratory.

An automatic sequential water sampler (Teledyne ISCO® 3700) containing 24 bottles of 1 litre capacity operated approximately 3 m above the intake of the pumping pipe according to the method described by Lewis (1996). The data logger triggered water sampling at regular intervals when turbidity critical thresholds (T1=5 g L^{-1} SiO_2 and T2=20 g L^{-1} SiO_2) were exceeded. Turbidity thresholds and sample frequency were adjusted according to SSC dynamics and seasonal variability. The vinyl pumping pipe was 5 m long and 9.5 mm in diameter; its intake was placed at a fixed height close to the turbidimeter, i.e. 20 cm from the river bottom. The pumping line was purged before and after each sample collection in order to limit self-contamination between successive samples. Given the high turbulence of the stream during flood events, samples were assumed to be representative of the flow across the full section.

Finally, precipitations were recorded with an automatic tipping bucket rain gauge (RainWise Rainew 111, 20.5 cm catch area), with a resolution of 0.254 mm per tip and connected to a data logger (Onset, Hobo Event). The gauge was installed at the centre of the catchment, in June 2008 at 1135 m ASL (Figure 1b).

2.3. Measurement of SSC

The one-litre water samples were processed in the laboratory using two different methods to estimate SSC (in g L^{-1}). The method based on the whole water sample was preferred to the method that uses sub-samples (or aliquot) in order to limit measurement bias associated with operator handling (Gray *et al.*, 2000). At low SSCs (estimated by expert judgment, <2 g L^{-1}), the whole sample volume was filtered through pre-weighed fibreglass Durieux filters (pore diameter, 0.7 µm), dried for 5 h at 105°C and then weighed again with a high precision scale. For higher SSCs (≥ 2 g L^{-1}), the whole sample volume (water and sediment) was settled; the SSC was estimated by weighing the sample after drying for 24 h at 105°C. SSC measurements refer to the total suspended sediment (i.e. including mineral and organic fractions). No measurement on organic fractions is available

for the Galabre catchment. Nevertheless, the organic carbon contents are generally lower than 1% in suspended sediments of alpine rivers draining areas with similar lithology and land use (Némery et al., 2013). Measurements of effective particle size distribution (PSD) were performed by Grangeon et al. (2012), using a specific protocol dedicated to samples with high levels of concentrations. The median diameters measured during five runoff events ranged from 5 to 39µm.

2.4. Data processing

2.4.1 Suspended sediment loads calculation

The turbidimeter was calibrated with SSC measurements of water samples collected during several floods. Calibration has been checked for each flood event since the installation of the turbidimeter based on the SSC measurements. The calibration protocol is detailed in Navratil *et al.* (2011). The turbidity-SSC calibration curve was restricted to the range of concentrations exceeding 0.2 g L^{-1}, because the sensor's ability to record very low concentrations appeared to be insufficient, which was already expected by the manufacturer. Although the standard relationship was reliable and applicable for most of the measuring period, turbidity-SSC hysteretic relationships (Lewis and Eads, 2008, Eder *et al.*, 2010) were observed during some flood events.

Suspended Sediment Discharges (SSD; expressed in [Mg s^{-1}]) were calculated as follows:

$$SSD(t) = Q(t) \cdot SSC(t) \cdot 10^{-3} \quad [1]$$

Suspended sediment yields, in Mg, could then be integrated at the desired time-scale(i) at the flood event (referred to as SSY_e), (ii) the annual or the inter-annual scales (i.e. SSY).

2.4.2 Flood event analyses

A total of 242 flood events were observed during the study period. Reliable water and suspended sediment data were collected for a total of 236 floods. Six events were excluded because of turbidity equipment malfunctioning. These events were characterised by low discharges (< 0.72 $m^3 s^{-1}$). All the flood events were considered in the current research. Floods were separated manually in time and relevant variables were estimated automatically using a program developed in R (http://www.r-project.org/). For these 236

flood events, the variables considered in the analysis were (i) the duration (Du, hours), (ii) the initial discharge at the start of the flood (Qi, $m^3 s^{-1}$), (iii) the peak discharge (Qx, $m^3 s^{-1}$), (iv) the total runoff volume (Qt, m^3), (v), the maximum suspended sediment concentration (SSCx, g L^{-1}), (vi) the estimated maximum suspended sediment discharge (SSDx, g s^{-1}), and (vii) the estimated suspended sediment yield (SSY_e, Mg). Since June 2008, 220 rainfall events were characterised, by considering (viii) the total precipitation depth during the event (Pt, mm), (ix) the maximum intensity of precipitation over a 10-min period (Ix10, mm h^{-1}), (x) the rainfall depth during the previous five days (P5d, mm), (xi) the total rainfall kinetic energy load (TKE, J m^{-2}), and (xii) the maximum kinetic energy of precipitation over a 10-min period (KEx10, J m^{-2} h^{-1}). These last characteristics were calculated using the exponential equation published by Foster (2004) for RUSLE2 (USDA-ARS, 2013) and based on rainfall intensity as follows:

$$KE10 = 29 \text{ x } [1 - 0.72 \exp(-0.082 \text{ x } I10)] \text{ x } I10 \qquad [2]$$

Where KE10 is the calculated rainfall kinetic energy (J m^{-2} h^{-1}) in 10 minutes and I10 is the rainfall intensity (mm h^{-1}) in 10 minutes.

For each storm event, an analysis of the relationship between SSC and discharge was conducted. Following the method proposed by Aich *et al*. (2014), normalized water discharges (noted Qn(i)) and SSC (noted SSCn(i)) were calculated according to respectively, the peak discharge (Qx) and the maximum SSC (SSCx) measured during the event. The discharge-SSC hysteresis loop patterns were classified into four different types based on their rotational direction using the conceptual approach initially proposed by Williams (1989). Three types of simple events were defined: clockwise, counter-clockwise and when the discharge and the SSC have simultaneous peaks (with no or light hysteresis). A fourth type corresponded to a more complex behaviour, very often characterised by the occurrence of multiple peaks.

2.5. Uncertainties

The uncertainties on SSC and SSY were estimated using the method proposed by Navratil *et al.* (2011) for the hydro-sedimentary station investigated in the current research.

Nine major uncertainty components associated with turbidity measurements were identified: the choice of the model of turbidimeter and its calibration; the temporal and spatial field sampling strategies; the technical problems during fieldwork; the river sampling; the laboratory sub-sampling and analysis; and finally, the discharge estimation.

SSC uncertainties remained on average lower than 10% for individual records (with a 95% confidence level), although they were highly variable, reaching up to ~70%. Uncertainties on flood indicators (SSCx) were close to 20% on average. Uncertainty of sediment yields at the flood event scale (SSY_e) amounted to about 15%, 19% and 29% depending on the level of uncertainty on discharge estimates: respectively 5%, for low discharges ($Q< 0.5\ m^3s^{-1}$), 10% for intermediate discharges ($0.5\ m^3\ s^{-1} < Q< 2.0\ m^3s^{-1}$) or 20% for high discharges ($Q> 2.0\ m^3\ s^{-1}$) (Sauer and Meyer, 1992; Baldassarre and Montanari, 2009 ; Navratil *et al.*, 2011).

The data set is available at https://bdoh.irstea.fr/DRAIX/.

3. RESULTS

3.1. High frequency data

Rainfall, discharge, SSC and SSD time-series are shown in Figure 2. Rainfall and discharge are characterised by a strong temporal variability and very wide ranges of variation. Figure 2a shows the rainfall distribution observed during the study period. During this period, 731 precipitation events with a total depth greater than 1 mm and 296 events with a total rainfall greater than 5 mm were recorded. 853 days (36 %) without rainfall were observed, and dry days with a total amount lower than 0.1 mm covered 63 % of the time. The maximum recorded instantaneous intensity was 216 mm h^{-1} corresponding to a maximum 103 mm h^{-1} rainfall intensity at a 10-min time step. The maximum daily precipitation was 94.2 mm (11/04/2014) and 12 days had more than 50 mm of rainfall.

During the measuring period we have not observed anomalies in the climatic records at the annual scale compared to the normal value calculated for a 30 years period (1985-2014). For example for precipitation amounts the annual values were in a range comprised between -12% (2011) and + 27 % (2013).

The discharge measured during the monitored period was characterized by a wide range of flow conditions (Figure 2b). The instantaneous discharge ranged from 0.007 $m^3\ s^{-1}$ to 34.0 $m^3\ s^{-1}$. The mean discharge was 0.281 $m^3\ s^{-1}$. The maximum daily discharge was

9.8 $m^3 s^{-1}$ (31/12/2009). Daily discharge exceeded 3.0 $m^3 s^{-1}$ during only 22 days whereas during 95 % of the time, discharge remained lower than 0.92 $m^3 s^{-1}$. The hydrological regime of the river is a typical Mediterranean mountain rainfall regime, with low flows occurring in summer, although flow remains perennial. The rainfall conditions explained the numerous fluctuations observed during the annual flow cycle. The floods typically occurred in spring following local thunderstorms whereas in autumn and winter they were the consequence of western and south-western depressions that produced moderate rainfall amounts with a homogeneous distribution across the catchment. With mean annual rainfall and discharge of 995 mm and 0.275 $m^3 s^{-1}$, respectively, the mean runoff coefficient amounted to 42.6 %. This high runoff coefficient is likely attributed to the karstic supply of groundwater originating from the limestone areas (Figure 1a) during summer (Abdelaziz and Bambi, 2016).

SSC were irregular and showed very high values (Figure 2c) without any clear seasonal tendency. During summer and autumn, runoff was limited but the production of suspended sediment by erosion was as important as in June and September. Mean SSC estimated as the average of all observations reached 0.45 g L^{-1}. Mean flood SCC, estimated as the mean of the measured concentrations during floods, was 3.95 g L^{-1}. The maximum SSC recorded during 10-minutes reached 361 g L^{-1} (09/09/2012) or 63.5 g L^{-1} when considering the daily value. Daily SSC exceeded 10 g L^{-1} during only 27 days, whereas during 95 % of time, it remained lower than 1.4 g L^{-1}.

Although the events leading to significant SSD occurred with an irregular frequency (Figure 2d), most of these events occurred late in autumn, in winter or early in summer (June). Mean SSD estimated as the mean of all observations was 0.41 kg s^{-1}. Mean flood SSD, estimated as the mean of the measured concentrations during floods, was 2.43 kg s^{-1}. The maximum SSD recorded during 10-minutes reached 1319 kg s^{-1} (23/06/2010) or 66.3 kg s^{-1} when considering the daily values. Daily SSD exceeded 10.0 kg s^{-1} during only 26 days whereas daily SSD was lower than 0.71 kg s^{-1} during 95 % of the time.

3.2. General description of flood events

SSC measured in all 801 samples collected in the river between 2007 and 2014 varied from 0.0 to 360.8 g L^{-1}, with a median value of 4.59 g L^{-1}. 32% of the samples had concentrations greater than 10 g L^{-1}. The corresponding water discharges were 0.016, 16.06, and 0.207 $m^3 s^{-1}$, respectively for the minimum, maximum and median values. Because of the high

353 scattering of the entire SSC - discharge dataset (Figure 3), no relationship was found
354 between flow discharge and SSC, although the latter varied by up to five orders of
355 magnitude. The highly variable and complex relationship complicated the drawing of any
356 rating curve. SSC spanned 3 orders of magnitude above a discharge of 1 $m^3 s^{-1}$, and 5 orders
357 below.

358 Among the 236 floods recorded, 66 (28%) occurred in spring, 52 (22%) in summer,
359 78 (33%) in autumn and 40 (17%) in winter. In the study area, floods may occur all
360 throughout the year. Given the large number of floods observed, it was impossible to
361 present the full flood dataset. Table 1 shows the characteristics of the 30 events that
362 recorded the higher SSY_e following a chronological order. The total contribution of these
363 events represented 81 % of the total sediment yield estimated for the entire study period.
364 Therefore, these 30 events were representative of the characteristics of the floods producing
365 most of the suspended sediment fluxes. Those parameters describing the rainfall
366 characteristics, the discharge, the SSC and the suspended sediment fluxes exhibited a wide
367 range of variations. This reflects the diversity of the processes that may occur within the
368 catchment during rainfall- runoff events, as some events characterised by high SSC but low
369 discharges (23/06/2010) can generate similar SSY as those events characterised by high
370 discharge and low maximum SSC (24/12/2009). In the same way, the comparison between
371 events occurring during similar periods (e.g. 23/06/2010 and 13/07/2011) and having
372 similar values of maximum SSC values can exhibit different discharge values, leading to
373 very different SSY. Accordingly, the singularity of each rainfall runoff event justifies the
374 need to analyse the hydrosedimentary processes over time-series that should be as long as
375 possible.
376
377 **4. DISCUSSION**
378
379 **4.1. Suspended sediment load assessment**
380
381 No relationship between SSC and flow discharge was found in the Galabre catchment
382 (Figure 3). This finding was confirmed whatever the time period considered, i.e. annual,
383 monthly (Figure 3), daily or even at the event scale. Therefore, it was impossible to estimate
384 sediment yields from flow discharges alone. This confirms the importance of using SSC
385 observations in combination with discharge values during each individual flood event to
386 obtain an accurate estimation of sediment loads in highly dynamic rivers as mentioned by

many authors (Williams, 1989; Lenzi and Marchi, 2000; Sadeghi *et al.*, 2008; Alexandrov *et al.*, 2009; Eder *et al.*, 2010; Gao and Josefson, 2012; Ziegler *et al.*, 2014; Tuset *et al.*, 2015) and by Navratil *et al.* (2011) in the study catchment. Nevertheless, despite this careful analysis, the calculated suspended sediment yield may not be representative of the inter-annual hydrosedimentary behaviour of the catchment, as a given measuring period might not be long enough to include the full diversity and range of intensities of the processes occurring in the region.

The average specific SSY (sSSY) estimated in the Galabre during the observation period was around 666 Mg km^{-2} Y^{-1}, which is an important value in comparison with values found in the literature. For comparison, the European alpine watersheds exhibit moderate values, varying typically between 500 and 1000 Mg km^{-2} Y^{-1} (Milliman and Syvitski, 1992). Mano *et al.* (2009) estimated an average sSSY of 615 and 592 Mg km^{-2} Y^{-1} on the Asse and Bléone catchments in Southern French Alps. Accordingly, the value found for the Galabre catchment in this study can be considered high when compared with catchments of similar size in the Alps region. Considering other catchments in the Mediterranean area also lead to the same conclusion. For instance in the Isábena watersheds the values ranged from 32 to 3651 Mg km^{-2} Y^{-1} (Francke *et al.*, 2014). In this work, the higher value was observed in areas characterised by extensive badlands that provide the main source of sediment (Lopez-Tarazon *et al.*, 2009). The sSSY found for the Galabre catchment is among the top ranked values analysed by Vanmaercke *et al.* (2011), using a large data set, to analyse regional variations of sSSY across Europe. It corresponds to the 0.97 percentile of the distribution under Mediterranean climate and for low mountain ranges (see Figure 6a and 6b). This value is even higher than the median estimated by Nadal-Romero *et al.* (2011) to around 600 Mg km^{-2} Y^{-1} for Mediterranean badlands catchments of the same size (see Figure 9 in Nadal-Romero *et al.* (2011)).

4.1.1 Interest of medium term data series to assess SS dynamics

In order to evaluate to which extent short pluri-annual time series (2 to 3 years) can provide a representative assessment of the suspended sediment fluxes for a given watershed, the medium term time series acquired over 7 years at the Galabre outlet were used to calculate the SSD, SSY and rainfall statistics over a 3-years sliding period (Table 2). Although the mean annual SSY and the characteristics of the rainfall events were rather similar from one period to the next, significant SSD and SSY variations occurred at the flood event scale.

The relative difference between the means calculated for a 3-year period or for the 7-year period reached on average 13%, 30% and 43% for the total rainfall, SSYe and SSDx, respectively. A similar result was found for the maximum values recorded for each period, as average relative variations amounted to 3%, 14% and 44% for the rainfall intensity, SSY and SSD. Accordingly, the comparisons made on the runoff event characteristics demonstrate that generalizing the results of a suspended sediment analysis conducted over a 3-years period may not be sufficient to capture the catchment behaviour to calculate representative inter-annual SS fluxes.

4.1.2 Interest of medium-term time-series to outline seasonality in SSY

The monthly SSY distribution was analysed first (Figure 4). Whatever the sub-period considered (Figure 4a to 4e), some months were characterized by very low and slightly dispersed SSY values. On the contrary, other months exhibited higher SSY median values with a large scattering. This latter finding remains in agreement with the previously mentioned singularity of each rainfall-runoff event that can lead to very different SSY despite their occurrence during a similar period. A second striking result is that the months characterized by large SSY were not necessarily the same from one 3-year period to the next. For instance, the examination of Figure 4a or Figure 4d may lead to different interpretations when trying to identify i) the periods of the main suspended sediment exports and ii) the processes responsible for erosion and sediment transport. Although it is clear that the monthly distribution of SSY during the 2007-2010 period showed a seasonal pattern, this pattern was not-well captured during the 2010-2013 nor the 2011-2014 periods. Variations in the seasonal distribution of SSY were even more striking in Figure 4f in which box plots include the events compiled over the entire 7 years period.

4.2. Factors explaining the seasonal behaviour of SSY

4.2.1. Characteristics of the periods exhibiting high SSY

The two main seasons for SSY transport occurred in spring and winter, as the months of June, November and December cumulated on average 64% of the total SS fluxes. Although these three months exhibited higher SSY than the rest of the year, their hydrosedimentary characteristics were different. As shown in Figure 3, the samples collected in June showed

higher SSC than those collected in November and December. SSC frequently reached 100 g L^{-1} in June while it remained generally one order of magnitude lower in winter. To the contrary, discharges were generally lower in June than in November and December (Figure 5).

The relationship between SSY_e and the TKE rainfall descriptor shows a rather high scattering (Figure 6a). Despite the difficulty to identify monthly trends, June may exhibit slightly higher rainfall energy on average than November and December. The relationship between SSY and the peak-flow (Q_x) was less scattered (Figure 6b), suggesting that the maximum discharge is the most relevant factor controlling the transport of suspended sediment as already outlined by Duvert *et al.* (2012). This was observed during all seasons, although June was likely characterized by lower SSY/Q_x ratios than November and December. This would suggest higher SSC occurring in June than early in winter, as already shown in Figure 3. Another common characteristic was the global shape of the $SSY\text{-}Q_x$ curve suggesting that the suspended sediment regime in this catchment was controlled by the discharge connecting sediment pathways between the hillslopes and the outlet, while the availability of sediment remained limited (i.e. supply-limited processes). Nevertheless it should be stressed that the low difference between June and November/December observed in the SSY-TKE relationship does not demonstrate neither a small impact of the rainfall energy on SSY, nor a small contrast in rainfall energy between these two crucial periods. Instead, it may indicate spatial variations in rainfall that could not be covered by the measuring station, particularly late in spring. Among the 236 flood events that occurred during the 7 years study period, due to the natural spatial patterns of precipitation, half of the precipitation events recorded by the rain gauge started after the record of the onset of discharge rising at the outlet. As mentioned by Mano *et al.* (2009) and Navratil *et al.* (2012), rainfall is characterized by important seasonal variations in this Alpine Mediterranean area, with two main contrasted regimes. Widespread rainfall events, with high cumulative amounts of low-intensity precipitation, occur early in winter while late spring is dominated by the occurrence of local and short (lasting for a few hours) convective storms with high rainfall intensities.

4.2.2. Processes controlling SSY in meso-scale Mediterranean Alpine catchment

Results shown in the previous section suggest that the two contrasted rainfall regimes

observed during the year could be associated with two contrasted hydrosedimentary behaviours in the catchment. First, June would be a period with extensive erosion of fine particles on hillslopes due to the occurrence of intense rainfall events with a rather limited transport capacity of the river flow, because of a decrease in the discharges (Figure 5). Then, November and December would be rather characterised by a high capacity of the river to export sediment due to the onset of a period with high discharges. During the second period, the availability of fine sediment would be the main factor limiting SSY (Figure 6b). Nadal-Romero et al. (2014) already pointed out such SSY seasonal variability in a small catchment (0.45 km²) in a Mediterranean mountain landscape. They linked the SSY seasonality to weather type occurrence in the catchment. Most of the sediment export occurs in autumn and are produced under SW airflow direction. Studies led in the Isabena river catchment (445 km²; eg. López-Tarazón *et al.*, 2012; Francke and López-Tarazón, 2014) also pointed out the importance of the weathering dynamics, the sediment exhaustion on the slopes and the seasonality of the temporary sediment storage in the riverbed. These processes lead to non-linear relationships between the flow discharge and sediment flux and thus to strong SSY seasonality at the outlet. This potential interpretation of the catchment behaviour and seasonality can be further discussed through the examination of the SSC-discharge hysteresis loops on the 236 flood events.

The percentage of flood events that exhibit the four types of loops defined in section 2.4.2 was calculated so as their contribution to the total suspended sediment yield during the observation period. Clockwise hysteretic floods, characterised by a maximum in SSC occurring before the peak flow, indicate a quick transfer of suspended sediment or the preferential mobilisation of sources located near the outlet or in the channel (Gellis, 2013). These floods represented 15 % of the events and produced 24 % of the total SSY (Figure 7a). They mainly occurred during winter and spring (Figure 7b). Counter-clockwise hysteretic floods, characterised by a maximum in SSC occurring after the peak flow, indicate a longer transfer of suspended sediment originating from hillslopes or river sections located far from the outlet. These floods were the most frequent although they were the least efficient to export SSY, in average 160 Mg km^{-2} per flood. They occurred mainly in summer and autumn. These floods represented 41 % of the events and produced 17 % of the total SSY. Simultaneous hysteretic floods were characterised by a maximum in SSC occurring at the same time as the peak flow, indicating a quick transfer of suspended sediment from sources that are well connected to the river network or located in the vicinity of the outlet. These floods represented 22 % of the events and produced 26 % of the total

SSY. They occurred mainly in summer and autumn. The last type of floods exhibited complex hysteretic loops with multiple SSC peaks occurring before or after the peak flows, indicating a heterogeneous spatial distribution of precipitation or the occurrence of heavy bursts of rainfall during the event. These floods represented 22 % of the events and produced 33 % of the total SSY. They occurred mainly in summer and autumn. Clockwise and complex hysteretic floods were the most efficient to export sediment from the catchment at the event scale, while complex floods contributed more to the total SSY over the long term (Figure 7a).

In the light of those characteristics, late spring and summer can be considered as periods with heavy thunderstorms generated floods with very high SSC (up to 100 g L^{-1}) although low to moderate peak-flow discharges. The transport capacity of the intermittent river network, i.e. the ephemeral network connecting gullies and badlands to the main river network, was assumed not to be sufficient to transport all the suspended sediment eroded from the hillslopes down to the main river network. As a result, an important proportion of this sediment may have deposited in the intermittent river network and could be easily available for remobilisation during autumn, winter and spring floods. Accordingly, late in autumn and in winter, the rainfall events are characterised by low to moderate rainfall intensities and they last for many hours or days, generating large cumulative rainfall amounts (Navratil *et al.*, 2012) and leading the system to reach a high level of hydrological connectivity. The amount of fine sediment stored in the intermittent river network during summer and early in autumn would then be progressively flushed until early spring as the discharges in the river remain rather high during this period (Figure 5). This overall behaviour could explain why a majority of counter-clockwise floods occur between July and October while clockwise floods mainly happen between November and May.

CONCLUSIONS

This study provided an original investigation of the relationship between rainfall, runoff and suspended sediment loads in a meso-scale Mediterranean mountainous catchment during an observation period covering seven years. The Galabre catchment is characterised by the occurrence of extensive soil erosion on hillslopes and the transport of massive volumes of sediment in the river network, generating higher values of suspended sediment yield that it could be expected when considering the relatively small size of the catchment.

Suspended sediment transport dynamics were strongly intermittent with the absence of clear relationships between rainfall, discharge and SSC. Nevertheless, the current research demonstrated the interest of obtaining medium-term time series. Accordingly, the hydro-sedimentary functioning of the catchment could not be captured when restricting the analysis to short time series of 2 or 3 years, despite the significant effort required for fieldwork. Analysing the variables recorded during the full 7-year period provided i) a representative assessment of the range of variations of suspended sediment fluxes at the event scale and ii) a clear description of the seasonality of SSY. This study highlighted in particular the temporal dis-connectivity occurring in meso-scale catchments over short time-scales (i.e. event or succession of events) between the meteorological forcing and the SSY at the outlet. The two crucial periods for suspended sediment transport at the outlet were June and November/December. The early summer period was characterised by a high SSC/discharge ratio, corresponding to the occurrence of intense events mobilising recently eroded sediments on hillslopes. In contrast, the early winter period was characterised by higher discharges connecting the whole hydrographic network, which led to the remobilisation of sediment and its transport to the outlet. These findings have crucial impacts for other studies to improve the future sediment modelling strategies, as obtaining satisfactory SSF simulations for a given event or period may strongly depend on the model parameterisation of the initial availability of sediment in the system and the modelling of the intermittent processes of suspended sediment deposition and re-suspension in the channel. These findings have also important operational implications, in order to predict and prevent the deleterious impacts of sediment fluxes on aquatic habitats, drinking or clean water supply to the hydroelectric power plants.

Acknowledgments

This work was part of the STREAMS (Sediment TRansport and Erosion Across Mountains) project, funded by the French National Research Agency (ANR/ BLAN06 - 1_13915. The Draix Bléone research observatory is also supported by CNRS INSU. The authors thank Fred Malinur and Lucas Muller for their technical assistance and their participation to the river monitoring. Finally, we would like to thank Jean Sébastien Moquet and an anonymous reviewer for their constructive comments.

589 **References**

590 Abdelaziz, R., Bambi, C.K.M., 2016. Groundwater Assessment of the Bleone Catchment
591 Karst Aquifer in Southern France. IOP Conference Series: Earth and Environmental
592 Science 44, 022028. doi:10.1088/1755-1315/44/2/022028

593 Aich, V., Zimmermann, A., Elsenbeer, H., 2014. Quantification and interpretation of
594 suspended-sediment discharge hysteresis patterns: How much data do we need? Catena
595 122, 120–129. doi:10.1016/j.catena.2014.06.020

596 Alexandrov, Y., Cohen, H., Laronne, J.B., Reid, I., 2009. Suspended sediment load, bed
597 load, and dissolved load yields from a semiarid drainage basin: A 15-year study. Water
598 Resources Research 45, 13. doi:10.1029/2008WR007314

599 Asselman, N.E.M., 1999. Suspended sediment dynamics in a large drainage basin: the
600 River Rhine. Hydrological Processes 13, 1437–1450.

601 Alvera, B., Garcia-Ruiz, J.M., 2000. Variability of Sediment Yield from a High Mountain
602 Catchment, Central Spanish Pyrenees. Arctic, Antarctic, and Alpine Research 32, 478.
603 doi:10.2307/1552397

604 Baldassarre G.B. and Montanari A., 2009 Uncertainty in river discharge observations: a
605 quantitative analysis Hydrology and Earth System Sciences Discussions, 6: 39–61.

606 Bogen J., Bønsnes T., 2005 The impact of hydropower development on the sediment budget
607 of the River Beiarelva, Norway. In: Walling DE, Horowitz AJ (eds) Sediment budgets
608 2. IAHS Publ. 292. IAHS, Wallingford, pp. 214–222

609 Brasington J. and Richards K., 2000. Turbidity and suspended sediment dynamics in small
610 catchments in the Nepal Middle Hills. Hydrological Processes 14: 2559-2574.

611 Coynel A., Schafer J., Hurtrez J.E., Dumas J., Etcheber H. and Blanc G., 2004. Sampling
612 frequency and accuracy of SPM flux estimates in two contrasted drainage basins, Science
613 of the Total Environment, 330: 233-247.

614 Cuomo, S., Della Sala, M., Novità, A., 2015. Physically based modelling of soil erosion
615 induced by rainfall in small mountain basins. Geomorphology 243, 106–115.
616 doi:10.1016/j.geomorph.2015.04.019
617 Dedkov, A.P., Moszherin, V.I., 1992. Erosion and sediment yield in mountain regions of
618 the world, in: IAHS Publication. Presented at the Erosion, debris flow and environment
619 in mountains regions, IAHS Press, Changdu, pp. 29–36.
620 Downing J., 2006. Twenty-five years with OBS sensors: The good, the bad, and the ugly.
621 Continental Shelf Research. 26: 2299–2318.
622 Duvert, C., Nord, G., Gratiot, N., Navratil, O., Nadal-Romero, E., Mathys, N., Némery, J.,
623 Regüés, D., García-Ruiz, J.M., Gallart, F., Esteves, M., 2012. Towards prediction of
624 suspended sediment yield from peak discharge in small erodible mountainous
625 catchments (0.45–22 km²) of France, Mexico and Spain. Journal of Hydrology 454-455,
626 42–55. doi.org/10.1016/j.jhydrol.2012.05.048
627 Eder, A., Strauss, P., Krueger, T., Quinton, J.N., 2010. Comparative calculation of
628 suspended sediment loads with respect to hysteresis effects (in the Petzenkirchen
629 catchment, Austria). Journal of Hydrology 389, 168–176.
630 doi:10.1016/j.jhydrol.2010.05.043
631 Evrard, O., Navratil, O., Ayrault, S., Ahmadi, M., Némery, J., Legout, C., Lefèvre, I.,
632 Poirel, A., Bonté, P., Esteves, M., 2011. Combining suspended sediment monitoring and
633 fingerprinting to determine the spatial origin of fine sediment in a mountainous river
634 catchment. Earth Surface Processes and Landforms 36, 1072–1089.
635 doi:10.1002/esp.2133
636 Foster I.D.L., Millington R. and Grew R.G., 1992. The impact of particle size controls on
637 stream turbidity measurements; Some implications for suspended sediment yield

638 estimation, in Erosion and Sediment Transport Monitoring Programmes in River Basins,
639 edited by J. Bogen, D. E. Walling, and T. J. Day, IAHS Publ. 210: 51-62.
640 Foster, G. R.: User's Reference Guide: Revised Universal Soil Loss Equation (RUSLE2),
641 US Department of Agriculture, Agricultural Research Service, Washington DC, 2004.
642 Francke, T., Werb, S., Sommerer, E., López-Tarazón, J.A., 2014. Analysis of runoff,
643 sediment dynamics and sediment yield of subcatchments in the highly erodible Isábena
644 catchment, Central Pyrenees. Journal of Soils and Sediments 14, 1909–1920.
645 doi.org/10.1007/s11368-014-0990-5.
646 Gao, P., Josefson, M., 2012. Event-based suspended sediment dynamics in a central New
647 York watershed. Geomorphology 139-140, 425–437.
648 doi:10.1016/j.geomorph.2011.11.007
649 Gaillardet J., Braud I., Hankard F., Anquetin S., Bour O., Dorfliger N., de Dreuzy J.R.,
650 Galle S., Galy C., Gogo S., Gourcy L., Habets F., Laggoun F., Longuevergne L.,
651 LeBorgne T., Naaim-Bouvet F., Nord G., Simonneaux V., Six D., Tallec T., Valentin C.,
652 Abril G., Allemand P., Arènes A., Arfib B., Arnaud L., Arnaud N., Arnaud P., Audry S.,
653 Bailly Comte V., Batiot C., Battais A., Bellot H., Bernard E., Bertrand C., Bessière H.,
654 Binet S., Bodin J., Bodin X., Boithias L., Bouchez J., Boudevillain B., Bouzou Moussa
655 I., Branger F., Braun J.J., Brunet P., Caceres B., Calmels D., Cappelaere B., Celle-
656 Jeanton H., Chabaux F., Chalikakis K., Champollion C., Copard Y., Cotel C., Davy P.,
657 Deline P., Delrieu, G., Demarty J., Dessert C., Dumont M., Emblanch C., Ezzahar J.,
658 Estèves M., Favier V., Faucheux M., Filizola N., Flammarion P., Floury F., Fovet O.,
659 Fournier M.31, Francez A. J.37, Gandois L.46 13 , Gascuel C., Gayer E., Genthon C.,
660 Gérard M.F., Gilbert D., Gouttevin I., Grippa M., Gruau G., Jardani A., Jeanneau L., Join
661 J.L., Jourde H., Karbou F., Labat D., Lagadeuc Y., Lajeunesse E., Lastennet R., Lavado
662 W., Lawin E., Lebel T., Le Bouteiller C., Legout C., Le Meur E., Le Moigne N., Lions

J., Lucas A., Malet J.P., Marais-Sicre C., Maréchal J.C., Marlin C., Martin P., Martins J., Martinez J.M., Massei N.31, Mauclerc A., Mazzilli N., Molénat, J., Moreira-Turcq P., Mougin E., Morin S., NdamNgoupayou J., Panthou G., Peugeot C., Picard G., Pierret M.C., Porel G., Probst A., Probst J.L., Rabatel A., Raclot D., Ravanel L., Rejiba F., René P., Ribolzi O., Riotte J., Rivière A., Robain H., Ruiz L., Sanchez-Perez J.M., Santini W., Sauvage S., Schoeneich P., Seidel J.L., Sekhar M., Sengtaheuanghoung O., Silvera N., Steinmann M., Soruco A., Tallec G., Thibert E., Valdes Lao D., Vincent C., Viville D., Wagnon P., Zitouna R. (2018) OZCAR: the French network of Critical Zone Observatories. Vadoze Zone Journal doi:10.2136/vzj2018.04.0067.

García-Ruiz, J.M., Arnáez, J., Beguería, S., Seeger, M., Martí-Bono, C., Regüés, D., Lana-Renault, N., White, S., 2005. Runoff generation in an intensively disturbed, abandoned farmland catchment, Central Spanish Pyrenees. CATENA 59, 79–92. doi:10.1016/j.catena.2004.05.006

Gellis, A. C. (2013), Factors influencing storm-generated suspended-sediment concentrations and loads in four basins of contrasting land use, humid-tropical Puerto Rico. Catena 104, 39-57. doi:10.1016/j.catena.2012.10.018.

Gourdin, E., Evrard, O., Huon, S., Lefèvre, I., Ribolzi, O., Reyss, J.-L., Sengtaheuanghoung, O., Ayrault, S., 2014. Suspended sediment dynamics in a Southeast Asian mountainous catchment: Combining river monitoring and fallout radionuclide tracers. Journal of Hydrology 519, 1811–1823. doi:10.1016/j.jhydrol.2014.09.056

Grangeon, T., Legout, C., Esteves, M., Gratiot, N., Navratil, O., 2012. Variability of the particle size of suspended sediment during highly concentrated flood events in a small mountainous catchment. Journal of Soils and Sediments 12, 1549–1558. doi:10.1007/s11368-012-0562-5

688 Gray J.R., Glysson G.D., Turcios L.M., and Schwarz G.E., 2000. Comparability of
689 Suspended-Sediment Concentration and Total Suspended Solids Data, U.S. Geological
690 Survey Water-Resources Investigations Report 00-4191, 14 p.
691 Gray J.R., and Gartner J.W., 2009. Technological advances in suspended-sediment
692 surrogate monitoring, Water Resour. Res., 45, W00D29, doi:10.1029/2008WR007063.
693 Korup, O., McSaveney, M.J., Davies, T.R.., 2004. Sediment generation and delivery from
694 large historic landslides in the Southern Alps, New Zealand. Geomorphology 61, 189–
695 207. doi:10.1016/j.geomorph.2004.01.001
696 Lee, C., Foster, G., 2013. Assessing the potential of reservoir outflow management to
697 reduce sedimentation using continuous turbidity monitoring and reservoir modelling.
698 Hydrological Processes 27, 1426–1439. doi:10.1002/hyp.9284
699 Lefrançois, J., Grimaldi, C., Gascuel-Odoux, C., Gilliet, N., 2007. Suspended sediment and
700 discharge relationships to identify bank degradation as a main sediment source on small
701 agricultural catchments. Hydrological Processes 21, 2923–2933. doi:10.1002/hyp.6509
702 Lenzi, M.A., Marchi, L., 2000. Suspended sediment load during floods in a small stream
703 of the Dolomites (northeastern Italy). Catena 39, 267–282.
704 Lenzi MA., Mao L. and Comiti F., 2003. Interannual variation of suspended sediment load
705 and sediment yield in an alpine catchment. Hydrological Sciences–Journal–des Sciences
706 Hydrologiques, 48 (6): 899-915.
707 Lewis J., 1996. Turbidity-controlled suspended sediment sampling for runoff-event load
708 estimation. Water Resources Research 32 (7): 2299-2310.
709 Lewis J. and Eads R., 2008. Implementation guide for turbidity threshold sampling:
710 principles, procedures, and analysis. Gen. Tech. Rep. PSW-GTR-212. Albany, CA: U.S.
711 Dep. of Agriculture, Forest Service, Pacific Southwest Research Station. 86 p.

López-Tarazón J.A., Batalla R.J., Vericat D. and Francke T., 2009, Suspended sediment transport in a highly erodible catchment: The River Isábena (Southern Pyrenees), Geomorphology, 109 (3-4): 210-221.

López-Tarazón, J.A., Batalla, R.J., Vericat, D., Balasch, J.C., 2010. Rainfall, runoff and sediment transport relations in a mesoscale mountainous catchment: The River Isábena (Ebro basin). Catena 82, 23–34. doi:10.1016/j.catena.2010.04.005

López-Tarazón, J.A., Batalla, R.J., 2014. Dominant discharges for suspended sediment transport in a highly active Pyrenean river. Journal of Soils and Sediments 14, 2019–2030. doi:10.1007/s11368-014-0961-x

Mano V., Némery J., Belleudy P. and Poirel A., 2009. Assessment of suspended sediment transport in four alpine watersheds (France): influence of the climatic regime, Hydrological Processes 22 doi : 10.1002/hyp.7178.

Meybeck M., Laroche L., Dürr H.H., Syvitski J.P., 2003. Global variability of daily Total Suspended Solids and their fluxes. Global Planetary Changes. 39: 65-93.

Milliman JD. and Syvitski JPM., 1992. Geomorphic/tectonic control of sediment discharge to the ocean: the importance of small mountainous rivers. The Journal of Geology, 100: 525-544.

Moatar F, Person G., Meybeck M., Coynel A., Etcheber H. and Crouzet P., 2006. The influence of contrasting suspended particulate matter transport regimes on the bias and precision of flux estimates. Science of the Total Environment, 370(2-3): 515- 531.

Morris, G.L., Fan, J. (Eds.), 1998. Reservoir sedimentation handbook: design and management of dams, reservoirs, and watersheds for sustainable use. McGraw-Hill, New York.

735 Morris, G., 2014. Sediment Management and Sustainable Use of Reservoirs, in: Wang,
736 L.K., Yang, C.T. (Eds.), Modern Water Resources Engineering, Handbook of
737 Environmental Engineering. Humana Press, pp. 279–337.
738 Nadal-Romero, E., Regüés, D., Latron, J., 2008. Relationships among rainfall, runoff, and
739 suspended sediment in a small catchment with badlands. Catena 74, 127–136.
740 doi:10.1016/j.catena.2008.03.014
741 Nadal-Romero, E., Martínez-Murillo, J.F., Vanmaercke, M., Poesen, J., 2011. Scale-
742 dependency of sediment yield from badland areas in Mediterranean environments.
743 Progress in Physical Geography 35, 297–332. doi.org/10.1177/0309133311400330
744 Nadal-Romero, E., Cortesi, N., González-Hidalgo, J.C., 2014. Weather types, runoff and
745 sediment yield in a Mediterranean mountain landscape. Earth Surface Processes and
746 Landforms 39, 427–437. doi:10.1002/esp.3451
747 Navratil, O, Esteves, M., Legout, C., Gratiot, N., Nemery, J., Willmore, S., Grangeon, T.,
748 2011. Global uncertainty analysis of suspended sediment monitoring using turbidimeter
749 in a small mountainous river catchment. Journal of Hydrology 398, 246–259.
750 Navratil, O., Evrard, O., Esteves, M., Legout, C., Ayrault, S., Nemery, J., Mate-Marin,
751 A., Ahmadi, M., Lefevre, I., Poirel, A., Bonte, P., 2012. Temporal variability of
752 suspended sediment sources in an alpine catchment combining river/rainfall monitoring
753 and sediment fingerprinting. Earth Surface Processes and Landforms 37, 828–846.
754 doi:10.1002/esp.3201
755 Némery, J. , Mano, V. , Coynel, A. , Etcheber, H. , Moatar, F. , Meybeck, M. , Belleudy,
756 P. and Poirel, A. (2013), Carbon and suspended sediment transport in an impounded
757 alpine river (Isère, France). Hydrol. Process., 27: 2498-2508. doi:10.1002/hyp.9387

Orwin J.F. and Smart C.C., 2004. Short-term spatial and temporal patterns of suspended sediment transfer in pro-glacial channels, Small River Glacier, Canada. Hydrological Processes. 18: 1521– 1542.

Owens PN., Batalla RJ., Collins AJ., Gomez B., Hicks DM., Horowitz AJ., Kondolf GM., Marden M., Page MJ., Peacock DH., Petticrew EL., Salomons W. and Trustrum NA., 2005. Fine-grained sediment in river systems: environmental significance and management issues. River Research and Applications 21: 693-717.

Park, J., Hunt, J.R., 2017. Coupling fine particle and bedload transport in gravel-bedded streams. Journal of Hydrology 552, 532–543. https://doi.org/10.1016/j.jhydrol.2017.07.023

Pfannkuche J. and Schmidt A., 2003. Determination of suspended particulate matter concentration from turbidity measurements: particle size effects and calibration procedures, Hydrol. Process. 17: 1951–1963.

Phillips J.M., Webb B.W., Walling D.E. and Leeks G.J.L., 1999. Estimating the suspended sediment loads of rivers in the LOIS study area using infrequent samples. Hydrological Processes 13: 1035–1050.

Regüés, D., Gallart, F., 2004. Seasonal patterns of runoff and erosion responses to simulated rainfall in a badland area in Mediterranean mountain conditions(Vallcebre, southeastern Pyrenees). Earth Surface Processes and Landforms 29, 755–767. doi:10.1002/esp.1067

Renwick, W.H., Smith, S.V., Bartley, J.D., Buddemeier, R.W., 2005. The role of impoundments in the sediment budget of the conterminous United States. Geomorphology 71, 99–111. doi:10.1016/j.geomorph.2004.01.010

Riley S.J., 1998. The sediment concentration-turbidity relation: its value in monitoring at Ranger Uranium Mine, Northern Territory, Australia. Catena 32: 1-14.

Sadeghi, S.H.R., Mizuyama, T., Miyata, S., Gomi, T., Kosugi, K., Fukushima, T., Mizugaki, S., Onda, Y., 2008. Determinant factors of sediment graphs and rating loops in a reforested watershed. Journal of Hydrology 356, 271–282. doi:10.1016/j.jhydrol.2008.04.005

Salant, N.L., Hassan, M.A., Alonso, C.V., 2008. Suspended sediment dynamics at high and low storm flows in two small watersheds. Hydrological Processes 22, 1573–1587. doi:10.1002/hyp.6743

Sauer V.B. and Meyer R.W., 1992. Determination of error individual discharge measurements, U.S. Geol. Surv. Open-File Rpt., 92-14.

Schmidt, K.-H., Morche, D., 2006. Sediment output and effective discharge in two small high mountain catchments in the Bavarian Alps, Germany. Geomorphology 80, 131–145. doi:10.1016/j.geomorph.2005.09.013

Skarbøvik, E., Stålnacke, P., Bogen, J., Bønsnes, T.E., 2012. Impact of sampling frequency on mean concentrations and estimated loads of suspended sediment in a Norwegian river: Implications for water management. Science of The Total Environment 433, 462–471. doi:10.1016/j.scitotenv.2012.06.072

Slaets, J.I.F., Schmitter, P., Hilger, T., Lamers, M., Piepho, H.-P., Vien, T.D., Cadisch, G., 2014. A turbidity-based method to continuously monitor sediment, carbon and nitrogen flows in mountainous watersheds. Journal of Hydrology 513, 45–57. doi:10.1016/j.jhydrol.2014.03.034

Stott T. and Mount N., 2007. Alpine proglacial suspended sediment dynamics in warm and cool ablation seasons: Implications for global warming. Journal of Hydrology 332(3-4): 259-270.

Thomas R.B. and Lewis J. 1993. A comparison of selection-at-list time and time-stratified sampling for estimating suspended sediment loads. Water Resources Research, 29(4): 1247–1256.

Tolorza, V., Carretier, S., Andermann, C., Ortega-Culaciati, F., Pinto, L., Mardones, M., 2014. Contrasting mountain and piedmont dynamics of sediment discharge associated with groundwater storage variation in the Biobío River. Journal of Geophysical Research: Earth Surface 119, 2730–2753. doi:10.1002/2014JF003105

Tropeano, D., 1991. High flow events and sediment transport in small streams in the "tertiary basin" area in piedmont (Northwest Italy). Earth Surface Processes and Landforms 16, 323–339. doi:10.1002/esp.3290160406

Turowski, J.M., Rickenmann, D., Dadson, S.J., 2010. The partitioning of the total sediment load of a river into suspended load and bedload: a review of empirical data: The partitioning of sediment load. Sedimentology 57, 1126–1146. doi:10.1111/j.1365-3091.2009.01140.x

Tuset, J., Vericat, D., Batalla, R.J., 2015. Rainfall, runoff and sediment transport in a Mediterranean mountainous catchment. Science of The Total Environment. doi:10.1016/j.scitotenv.2015.07.075

USDA-ARS, 2013. Revised Universal Soil Loss Equation (RUSLE 2). Sci. Doc. USDA-Agric. Res. Serv. 2, 1–355.

Valero-Garcés, B.L., Navas, A., Machín, J. and Walling, D., 1999. Sediment sources and siltation in mountain reservoirs: a case study from the central Spanish Pyrenees. Geomorphology **28**: 23–41.

Vanmaercke, M., Poesen, J., Verstraeten, G., de Vente, J., Ocakoglu, F., 2011. Sediment yield in Europe: Spatial patterns and scale dependency. Geomorphology 130, 142–161. doi:10.1016/j.geomorph.2011.03.010

831 Vanmaercke, M., Poesen, J., Radoane, M., Govers, G., Ocakoglu, F., Arabkhedri, M., 2012.
832 How long should we measure? An exploration of factors controlling the inter-annual
833 variation of catchment sediment yield. Journal of Soils and Sediments 12, 603–619.
834 doi:10.1007/s11368-012-0475-3.
835 Walling, D.E., Moorehead, P.W., 1989. The particle size characteristics of fluvial
836 suspended sediment: an overview. Hydrobiologia 176/177, 125–149.
837 Walling, D.E., Fang, D., 2003. Recent trends in the suspended sediment loads of the world's
838 rivers. Global and Planetary Change 39, 111–126. doi:10.1016/S0921-8181(03)00020-1
839 Wass, P.D., Leeks, G.J.L., 1999. Suspended sediment fluxes in the Humber catchment, UK.
840 Hydrol. Process. 13, 935–953. doi:10.1002/(SICI)1099-1085(199905)13:7<935::AID-
841 HYP783>3.0.CO;2-L
842 Williams, G.P., 1989. Sediment concentration versus water discharge during single
843 hydrologic events in rivers. Journal of Hydrology 111, 89–106.
844 Wood P.J. and Armitage P.D., 1997. Biological effects of fine sediment in the lotic
845 environment. Environmental Management **21**: 203–217.
846 Wren D.G., Barkdoll B.D., Kuhnle R.A. and Derrow R.W., 2000. Field techniques for
847 suspended sediment measurement. Journal of Hydraulic Engineering, **126**(2): 97–104.
848 Zabaleta, A., Martínez, M., Uriarte, J.A., Antigüedad, I., 2007. Factors controlling
849 suspended sediment yield during runoff events in small headwater catchments of the
850 Basque Country. Catena 71, 179–190. doi:10.1016/j.catena.2006.06.007
851 Ziegler, A.D., Benner, S.G., Tantasirin, C., Wood, S.H., Sutherland, R.A., Sidle, R.C.,
852 Jachowski, N., Nullet, M.A., Xi, L.X., Snidvongs, A., Giambelluca, T.W., Fox, J.M.,
853 2014. Turbidity-based sediment monitoring in northern Thailand: Hysteresis, variability,
854 and uncertainty. Journal of Hydrology 519, 2020–2039.
855 doi:10.1016/j.jhydrol.2014.09.010

Tables and Figures Captions

Table 1: General characteristics of the 30 events with the highest suspended sediment yields in the Galabre catchment. These 30 main events account for 81 % of the total suspended sediment yield over the 2007-2014 study period. The event scale characteristics correspond to: Duration of the event (Du) (hours), Initial discharge (Qi) (m3 s^{-1}), Maximum discharge (Qx) (m^3 s^{-1}), Total runoff volume (Qt) (m^3), Max. suspended sediment concentration (SSCx) (g L^{-1}), Max. suspended sediment discharge (SSDx) (Kg s^{-1}), Suspended sediment yield (SSYe) (Mg), Total precipitation depth (Pt) (mm), Maximum 10 min rainfall intensity (Ix10) (mm h^{-1}), Rainfall depth during the 5 previous days (P5d) (mm), Total rainfall kinetic energy (TKE) (J m^{-2}), Maximum rainfall kinetic energy (KEx) (J m^{-2} h^{-1}), Hysteresis type (Cc counterclockwise, Si simultaneous, Cw clockwise, Co complex).

Table 2: Annual Suspended Sediment Yields (SSY) (Mg) and three hydrosedimentary characteristics computed at the rainfall-runoff event scale in the Galabre catchment. Statistics were processed for the entire period (2007-2014) and for five 3 year periods (hydrological years). The three event scale characteristics correspond to the Maximum Suspended Sediment Discharge (SSDx) (Kg s^{-1}), the Suspended Sediment Yield (SSYe) (Mg), and the Total Precipitation depth (Pt) (mm).

Figure 1: The Galabre River at La Robine in the Southern French Prealps. (a) Study area location in the Bléone River basin. (b) Geological map, (c) Land use map.

Figure 2: Seven-year monitoring of hydrosedimentary characteristics of the Galabre catchment from October 2007 to December 2014. (a) Rainfall intensity (mm h^{-1}) at Ainac

site, (b) river discharges (m^3 s^{-1}), (c) Suspended Sediment Concentrations (g L^{-1}), (d) Suspended Sediment Discharges (Kg s^{-1}).

Figure 3: Scatter plot showing the relationship between discharges and SSC measured on 801 samples at the Galabre River outlet for the 7-year study period.

Figure 4: Box plots showing the distribution of monthly suspended sediment yields calculated over various three year sliding periods and over the entire 7-year study period.

Figure 5: Box plots showing the distribution of monthly discharge over the 7-year study period.

Figure 6: Scatter plot showing the relationship between Suspended Sediment Yield at the outlet of the Galabre catchment with a) the total rainfall kinetic energy and b) the maximum discharge. The red and blue lines correspond to power law fitting curves for June and November-December data, respectively.

Figure 7: Distribution of the discharge SSC hysteretic loop types according to a) their number or contribution to the total SSY, and b) the month during hydrological years.

Figure

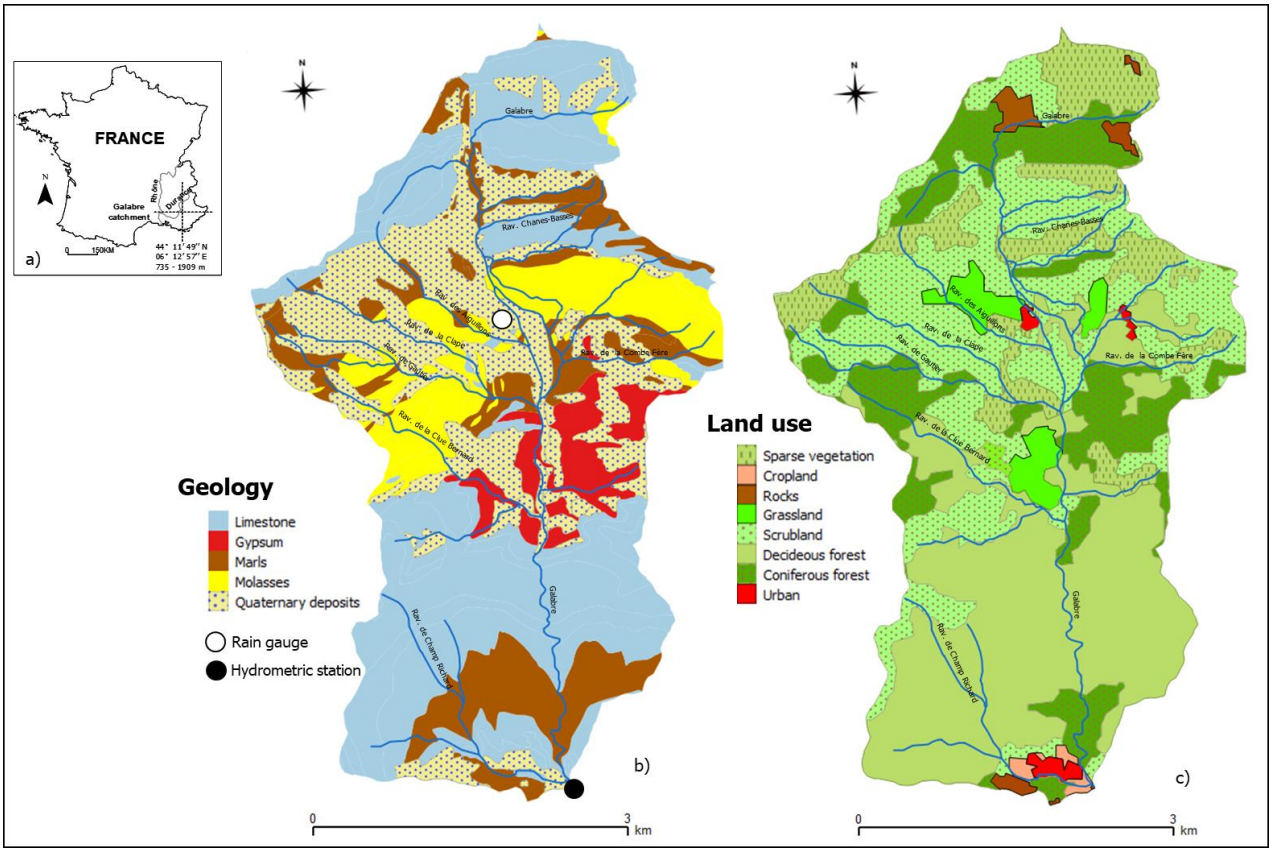

Figure 1:

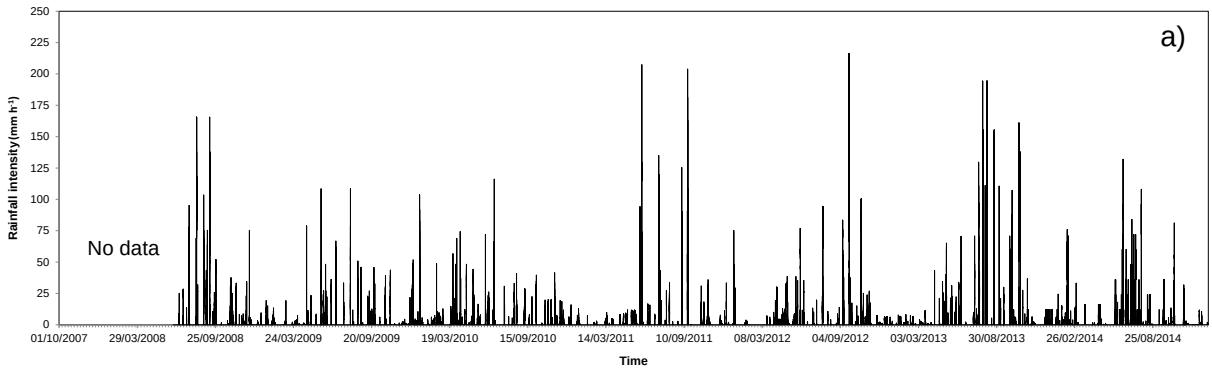
a)
Rainfall intensity (mm h-1)
No data
250
225
200
175
150
125
100
75
50
25
0
01/10/2007
29/03/2008
25/09/2008
24/03/2009
20/09/2009
19/03/2010
15/09/2010
14/03/2011
10/09/2011
08/03/2012
04/09/2012
03/03/2013
30/08/2013
26/02/2014
25/08/2014
Time

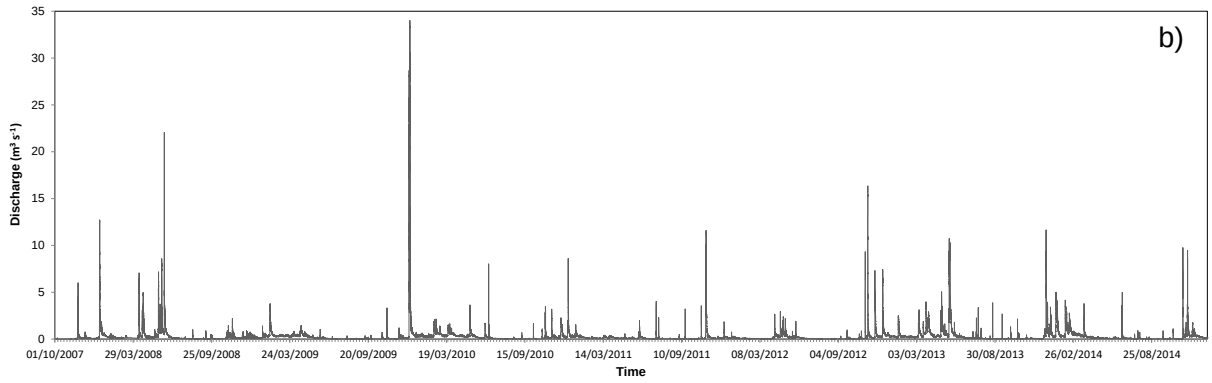
b)
Discharge (m3 s-1)
35
30
25
20
15
10
5
0
01/10/2007
29/03/2008
25/09/2008
24/03/2009
20/09/2009
19/03/2010
15/09/2010
14/03/2011
10/09/2011
08/03/2012
04/09/2012
03/03/2013
30/08/2013
26/02/2014
25/08/2014
Time

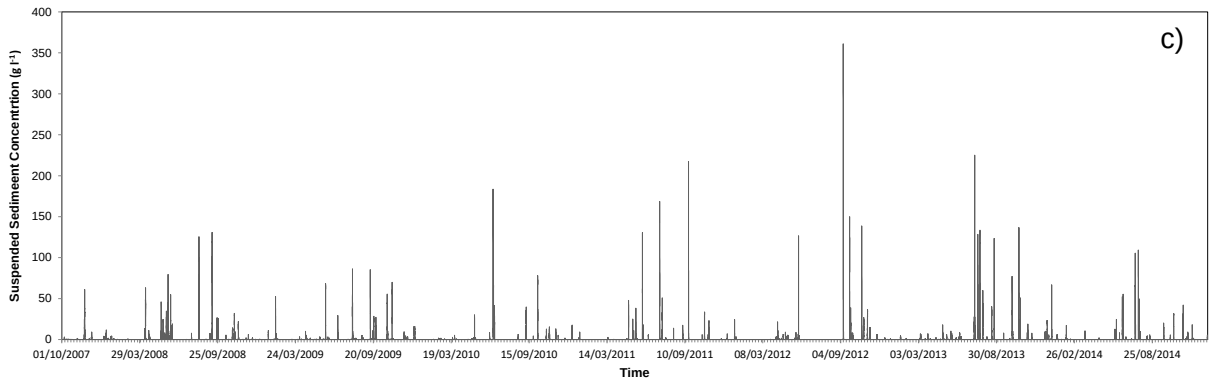
c)
Suspended Sediment Concentrtion (g l-1)
400
350
300
250
200
150
100
50
0
01/10/2007
29/03/2008
25/09/2008
24/03/2009
20/09/2009
19/03/2010
15/09/2010
14/03/2011
10/09/2011
08/03/2012
04/09/2012
03/03/2013
30/08/2013
26/02/2014
25/08/2014
Time

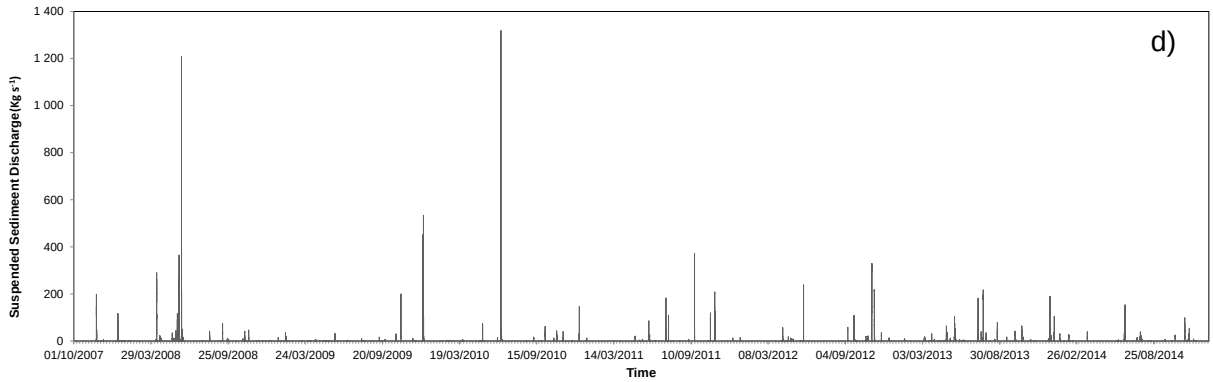
d)
Suspended Sediment Discharge (Kg s-1)
1 400
1 200
1 000
800
600
400
200
0
01/10/2007
29/03/2008
25/09/2008
24/03/2009
20/09/2009
19/03/2010
15/09/2010
14/03/2011
10/09/2011
08/03/2012
04/09/2012
03/03/2013
30/08/2013
26/02/2014
25/08/2014
Time

Figure 2:

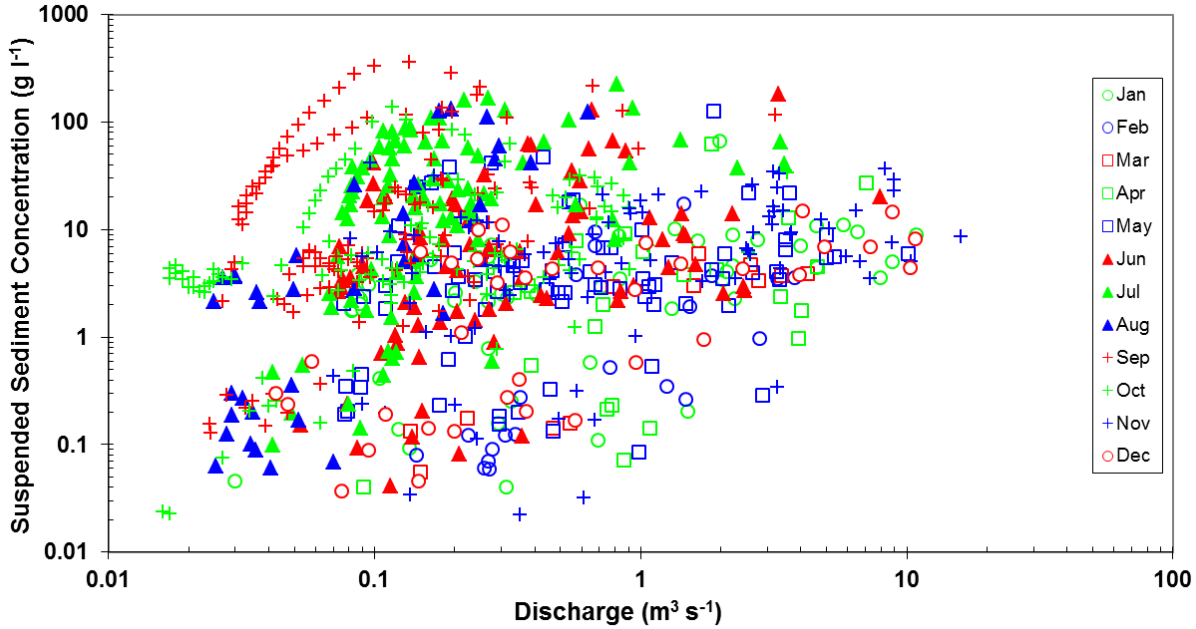

Figure 3:

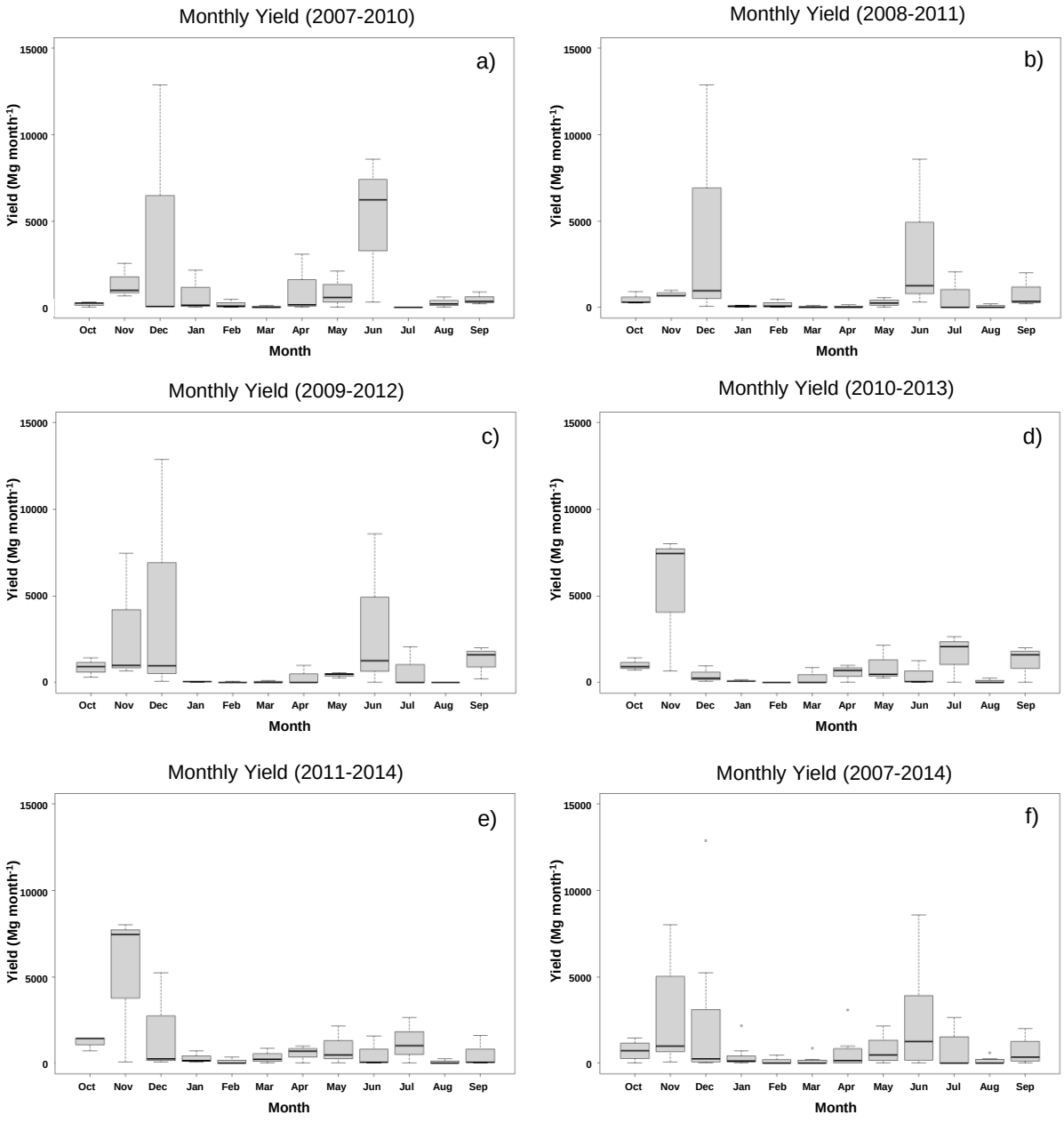
Monthly Yield (2007-2010)
a)
Monthly Yield (2008-2011)
b)
Monthly Yield (2009-2012)
c)
Monthly Yield (2010-2013)
d)
Monthly Yield (2011-2014)
e)
Monthly Yield (2007-2014)
f)
Yield (Mg month-1)
15000
10000
5000
0
Oct
Nov
Dec
Jan
Feb
Mar
Apr
May
Jun
Jul
Aug
Sep
Month

Figure 4:

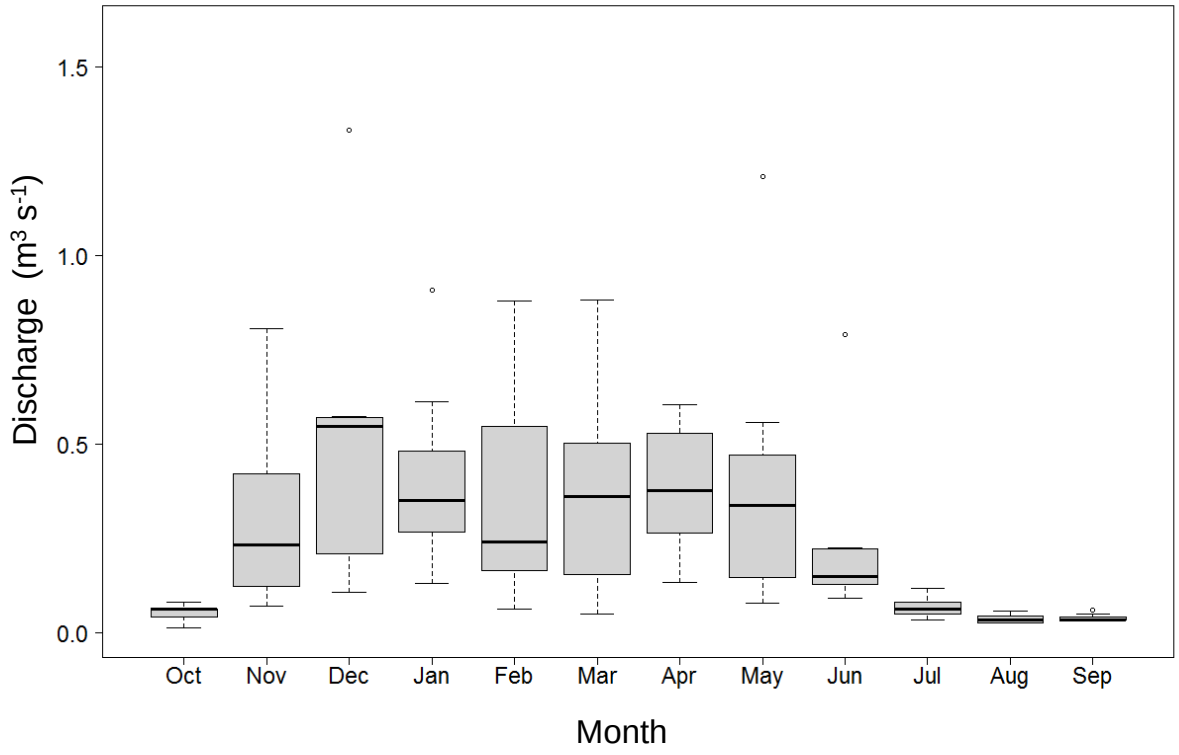
Discharge (m3 s-1)
1.5
1.0
0.5
0.0
Oct
Nov
Dec
Jan
Feb
Mar
Apr
May
Jun
Jul
Aug
Sep
Month

Figure 5:

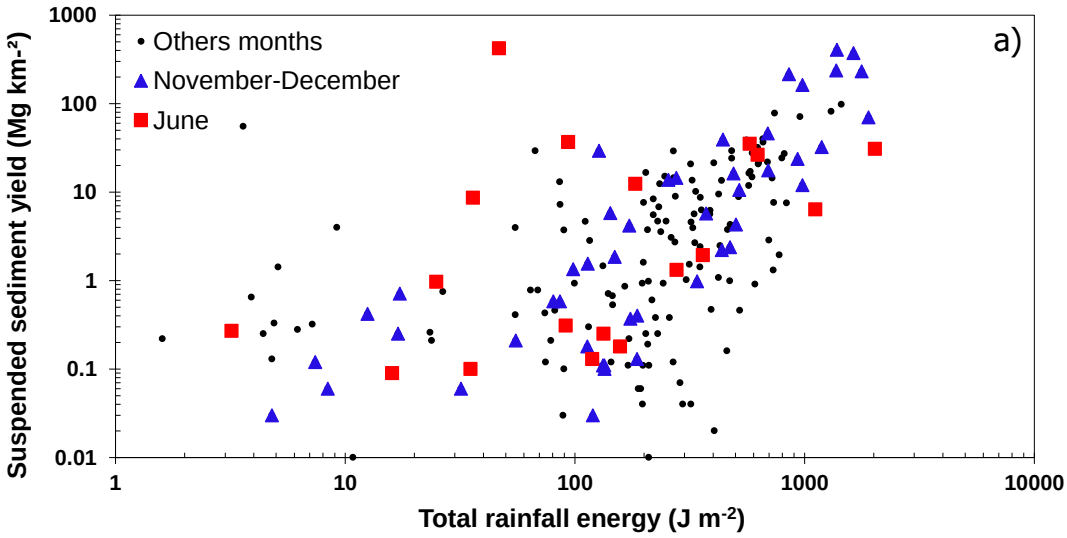
a)
Others months
November-December
June
Suspended sediment yield (Mg km-2)
Total rainfall energy (J m-2)
1000
100
10
1
0.1
0.01
1
10
100
1000
10000

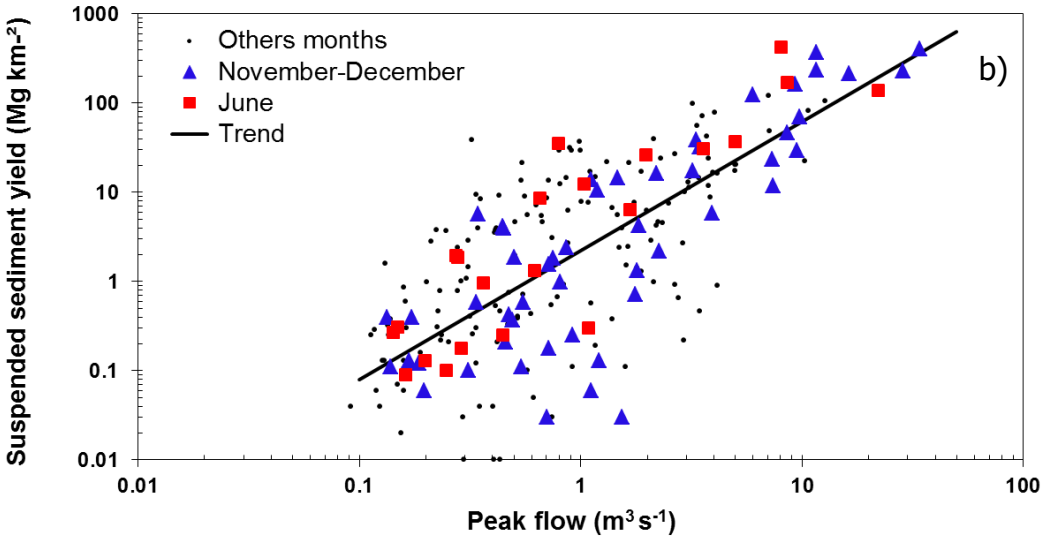
b)
Others months
November-December
June
Trend
Suspended sediment yield (Mg km-2)
Peak flow (m3 s-1)
1000
100
10
1
0.1
0.01
0.01
0.1
1
10
100

Figure 6 :

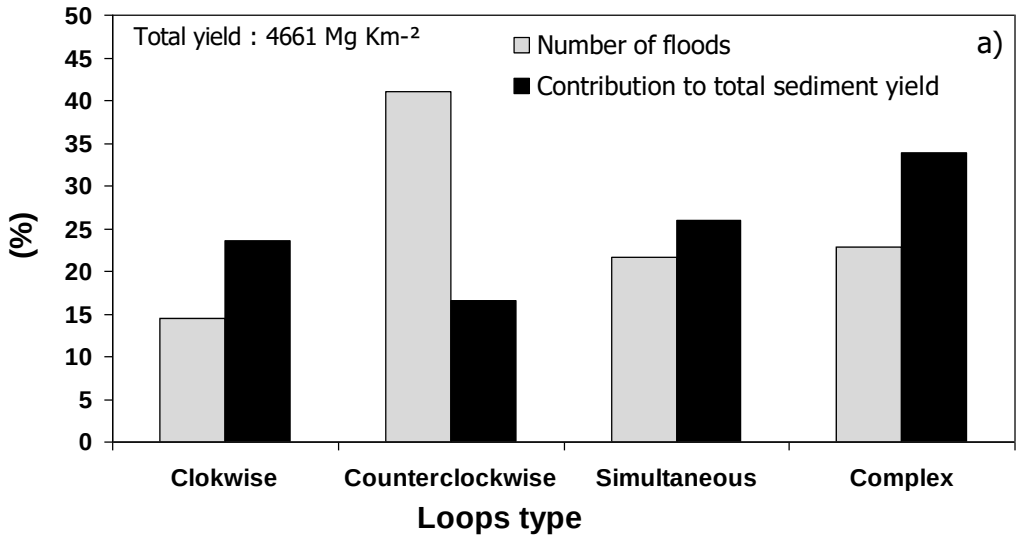
Total yield : 4661 Mg Km-2
Number of floods
Contribution to total sediment yield
a)
(%)
50
45
40
35
30
25
20
15
10
5
0
Clokwise
Counterclockwise
Simultaneous
Complex
Loops type

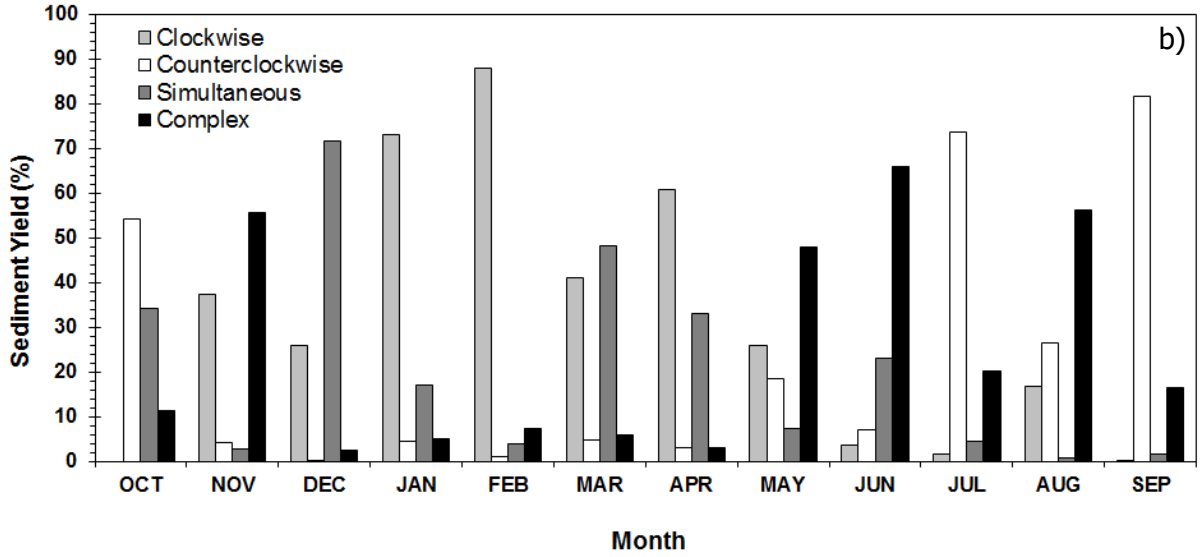
Clockwise
Counterclockwise
Simultaneous
Complex
b)
Sediment Yield (%)
100
90
80
70
60
50
40
30
20
10
0
OCT
NOV
DEC
JAN
FEB
MAR
APR
MAY
JUN
JUL
AUG
SEP
Month

Figure 7:

Table 1

Flood date	Du	Qi	Qx	Qt	SSCx	SSDx	SSY_e	Pt	Ix10	P5d	TKE	KEx10	Hystr
22/11/2007	63.8	0.220	6.00	316 448	61.1	198.1	2 484	--	--	--	--	--	Co
10/01/2008	88.7	0.101	12.71	791 770	11.6	116.6	2 090	--	--	--	--	--	Cw
11/04/2008	54.0	0.274	7.06	254 138	63.2	290.2	2 442	--	--	--	--	--	Cw
24/05/2008	95.5	0.261	7.16	579 761	8.2	43.3	982	--	--	--	--	--	Cw
29/05/2008	82.0	0.727	3.72	464 908	34.7	115.7	857	--	--	--	--	--	Co
01/06/2008	93.7	0.690	8.57	643 190	79.3	364.5	3 415	--	--	--	--	--	Co
08/06/2008	76.7	0.506	22.05	603 841	54.8	1209.0	2 791	--	--	--	--	--	Si
11/09/2008	28.7	0.045	0.89	14 401	130.7	74.1	636	26.5	46.6	11.5	624.7	1330.5	Cc
01/11/2009	51.0	0.031	3.32	36 596	69.9	199.3	782	28.8	24.2	0	441	633.6	Cc
22/12/2009	33.5	0.187	28.66	847 152	16.0	450.7	4 636	107.9	15.3	2.3	1772.1	352.7	Si
24/12/2009	26.2	3.632	34.00	1 443 107	16.0	534.4	8 131	80.4	17.4	114.1	1382.5	417.4	Si
23/06/2010	94.7	0.131	8.01	204 157	183.4	1318.7	8 457	3.6	5.8	7	46.7	93.4	Co
30/10/2010	165.0	0.064	3.46	293 578	15.3	42.9	645	80.6	12.2	52.2	1187.1	261.3	Co
21/12/2010	180.2	0.189	8.59	649 964	17.6	145.5	921	52.8	9.9	10.5	691.8	195.3	Si
03/06/2011	18.5	0.081	0.80	18 752	130.4	85.3	705	28.1	32.2	27.5	577.6	886.4	Si
13/07/2011	37.8	0.043	4.03	29 542	168.6	182.5	1 562	33.4	47.4	0.4	740.6	1354.2	Cc
18/09/2011	39.8	0.071	3.21	22 924	217.0	372.2	1 964	60.2	57.2	10.7	1445.9	1647.4	Cc
24/10/2011	111.5	0.047	3.55	99 634	33.5	118.9	1 425	64.2	10.8	13.8	956.9	220.2	Si
03/11/2011	159.7	0.095	11.59	1 185 084	23.0	207.8	7 433	108.4	18.5	12.9	1634.3	451.1	Co
09/09/2012	40.2	0.027	0.32	7 498	360.8	57.9	775	22.5	35.4	0.3	559.3	985.9	Cc
24/09/2012	38.0	0.027	0.99	9 998	150.0	108.6	733	24	103.3	0.1	661.1	2996.3	Co
04/11/2012	40.7	0.058	9.32	194 455	36.5	329.6	3 235	61.4	17	5	979.5	406.2	Cw
09/11/2012	102.0	0.132	16.35	899 203	14.6	218.1	4 290	63.4	10.1	62.6	855.4	201.9	Cw
15/05/2013	62.5	0.246	10.73	847 268	10.2	94.6	1 631	89.5	12.4	14	1306.3	266.5	Co
22/07/2013	15.7	0.087	3.35	23 535	133.6	216.8	1 106	0.4	0.5	36.5	3.6	4.3	Cc
20/10/2013	30.3	0.044	2.15	16 328	136.6	63.3	796	26.5	75.1	1.4	659	2173.7	Cc
25/12/2013	77.3	0.359	11.64	889 114	23.2	190.2	4 740	92.1	10.4	59.9	1373.9	208.5	Cw
17/06/2014	24.0	0.088	3.57	56 672	35.4	120.3	615	77.3	84	17.2	2023.6	2434.3	Si
18/06/2014	14.7	0.302	4.97	48 789	55.3	141.0	738	6	7.2	96.6	93.4	125.5	Cc
04/11/2014	56.8	0.040	9.75	295 269	42.1	99.9	1 398	99.1	23.2	4.2	1899.7	599.1	Co

Table 2

SSY	2007-2010	2008-2011	2009-2012	2010-2013	2011-2014	2007-2014[a]
Total by period	43 030	35 594	43 042	36 158	38 703	89 993
Mean annual	14 343	11 865	14 347	12 052	12 901	12 856
SSDx						
Minimum	0.0	0.1	0.0	0.0	0.0	0.0
Maximum	1318.7	1318.7	372.2	329.6	329.6	1318.7
Mean	74.1	74.8	36.7	31.6	28.3	45.6
Median	4.4	3.3	3.6	3.9	4.8	4.4
Std. Dev.	223.0	210.2	72.1	64.6	56.7	139.5
SSYe						
Minimum	0	1	0	0	0	0
Maximum	8 457	8 457	7 433	7 433	4 740	8 457
Mean	590	625	369	357	286	408
Median	57	44	39	29	30	48
Std. Dev.	1 543	1 728	1 057	1 042	753	1 146
Pt						
Minimum	0.0	0.0	0.0	0.0	0.0	0.0
Maximum	107.9	107.9	108.4	108.4	92.1	108.4
Mean	23.4	27.5	22.9	20.1	18.5	21.1
Median	17.1	23.9	15.6	12.5	12.2	15.5
Std. Dev.	20.4	23.2	21.2	23.2	21.7	21.2

[a] Average value for the study period